Electric Power Systems Research 234 (2024) 110516

Contents lists available at ScienceDirect

Electric Power Systems Research

journal homepage: www.elsevier.com/locate/epsr

Applying shape of current traveling waves for transmission line protection

Kuldip Nayak *, Soumitri Jena, Ashok Kumar Pradhan

Department of Electrical Engineering, Indian Institute of Technology Kharagpur, 721302, West Bengal, India

ARTICLE INFO

Keywords:
Line protection
Traveling wave
Waveshape
Wave propagation
Wave distortion

ABSTRACT

This paper leverages the shape of current traveling waves to enhance transmission line protection. It investigates the distortion effect on the traveling waveshape during propagation along the transmission line. It focuses on utilizing the ratio of area to the peak of the initial traveling wave at the local end to estimate the level of distortion and identify faults within the protection zone. This eliminates the need for arrival time information of initial waves, detection of subsequent traveling waves, and synchronized data communication from the remote end. Effectiveness of the proposed method is evaluated through simulations of faults in a 400 kV transmission network and real-time testing on the RTDS Novacor simulator. The ratio of area and peak, being less affected by the fault resistance and variation in inception angle, the proposed method offers more reliability for traveling wave-based line protection compared to available techniques.

1. Introduction

Traveling waves (TWs) originate due to sudden changes in voltage in a power network. As a function of space and time, these electromagnetic waves initiated during fault carry information about the type of fault, its location, and direction [1]. They arrive at the line ends within few microseconds, thereby making high-speed protection possible [2,3]. Fast and reliable fault detection is essential to reduce the fault clearance time, which improves the transient stability of high-voltage power systems [3]. Different TW-based relays use either one or both end data for line protection and fault location.

1.1. Literature analysis

The TW-based current differential protection in [3] uses data from both ends of a line to calculate the operating and restraining quantities. The method eliminates the high-fidelity voltage requirement for identifying internal and external faults; however, the implementation requires high-speed communication channels and data synchronization. There are several practical challenges with data synchronization and communication at such high sampling rates [4]. The feasibility of employing two-terminal traveling wave-based protection at low sampling frequencies has been proposed in [5]. The communication bandwidth requirement is reduced in the differential protection scheme reported in [6,7]. However, the reconstruction of current TWs from wavelet transform maxima is required at the line ends, which involves complex computation and may burden the microprocessor relays. The transmission line protection scheme proposed in [8] uses mathematical morphology to extract the polarity and time of arrival (ToA) of initial current TWs from both ends. The scheme needs reduced communication bandwidth, but the issues with time-synchronized data and complex computation persist. The requirement of time-synchronized data is eliminated in the method of [9] by using fixed latency communication channels. It requires precise ToA estimation at both ends of the line, which may not be feasible in case a highly dispersed signal is received at the relay location. The accuracy in ToA estimation also depends on the efficacy of the interpolation method used in the algorithm [10].

Performance of one-ended and two-ended traveling wave fault location techniques in series compensated transmission lines, emphasizing the influence of series capacitors and their overvoltage protection has been discussed in [11]. Impact of different correlation functions, filtering techniques, and observation window lengths on fault location accuracy in single-ended correlation-based traveling wave fault location algorithms has been proposed in [12]. A two-terminal traveling-wave-based protection algorithm tailored for non-homogeneous transmission lines, addressing close-in faults and sampling rate effects has been presented in [13]. In [14] a new approach to mitigate uncertainties in line propagation velocity and travel time of TW fault location estimations using real-world TW records has been presented. The line protection technique in [15] uses the direction information from both end to identify internal faults, and only the decisions are communicated. Thereby, the need for high-bandwidth communication is reduced. However, unlike distance protection schemes [16], trip decision cannot be made in case of communication failure. Impact of communication channel

* Corresponding author.
E-mail address: lucky.kuldip@gmail.com (K. Nayak).

https://doi.org/10.1016/j.epsr.2024.110516
Received 30 December 2023; Received in revised form 26 April 2024; Accepted 26 May 2024
Available online 12 June 2024

latency on TW based line protection functions has been highlighted in [17]. A practical solution for TW-based fault location with limited sampling rates, extending its practicality has been provided in [18]. TW-based distance protection element reported in [16,19] uses the difference in propagation velocity of first incident alpha and zero-mode current TWs to estimate the fault distance. Higher attenuation in zero-mode of propagation affects the performance of such a method during remote faults [20,21], and the application is limited to ground faults only. The online fault location methods in [22,23] have application scope for TW-based distance relaying. The methods in [22,23] utilize the incident and successive reflected current TWs at one end to determine the fault distance. However, the identification of the point of TW reflection, (*i.e.* the fault point or remote terminals) is challenging. Further, the reflected wave magnitudes are significantly lower and may be unsuitable for fault location.

1.2. Research gaps

In summary,

- Contemporary TW-based protection methods heavily rely on synchronized TW data precise from line terminals and precise TW arrival time estimation. However, the complexities associated with data synchronization and communication at high sampling rates are challenging.
- Single-ended traveling wave (TW) distance protection methods encounter challenges in distinguishing reflected waves from various transition points, including line terminals, adjacent lines, or fault points. Alternatively, utilizing only initial traveling waves limits applicability of the methods to only ground faults.

These above challenges necessitate the development of a single-ended TW-based line protection method without analyzing the subsequent reflected TWs.

1.3. Statement of problem

The double-ended current TW-based methods face challenges regarding precise arrival time estimation, compounded by practical difficulties in data synchronization and communication at high sampling rates for protection applications, particularly for close-in faults. Hence, there is a need for a simplified, single-ended TW-based distance protection method to address these limitations and ensure reliable and efficient line protection. Further, the single-ended line protection method should utilize only initial TWs and be applicable for all the fault types.

A transmission line protection using the information extracted from the waveshape of incident current TW at the local end is proposed in this paper. The ratio of area under the waveshape and peak is utilized with directional supervision at the corresponding end to identify internal faults in the protected line. Remote end current data and identification of subsequent TWs reflected from the fault point, remote terminal, or adjacent line terminal are not required in the proposed method. Fault distance estimation using the area and peak of waveshape, introduced in the proposed method, is not altered by the fault resistance and variation in fault inception angle. The uniqueness of the proposition comprises,

1. The method utilizes the information based on the distortion on the waveshape of the current TW introduced due to the propagation in the line.
2. The zone boundary has been defined in terms of the ratio of area under the waveshape and peak, which is less affected by the fault parameters.
3. It uses only the initial waves; thereby, the problem of identifying the reflected TW from the fault point or remote bus is avoided.

In a 400 kV transmission network and a real-time simulation environment, the proposed technique is found to be dependable for a broad range of internal faults and stable during external faults. Comparative analysis with available TW-based protection highlights its advantages.

2. Background theory

2.1. TW propagation

A network fault results in an abrupt voltage dip at the fault location [24]. For example, a fault of zero resistance results in a voltage change from the pre-fault value to near zero volts. This sharp voltage change launches current TWs at the fault location that propagate towards the line terminals. The current TW propagation in a transmission line is expressed in the Laplace domain as [25],

$$I(x,s) = I_I e^{-\gamma(s)x} + I_R e^{\gamma(s)x} \tag{1}$$

where I_I and I_R incident and reflected TWs, respectively. x is the propagated distance. The propagation constant (γ) is given by [25],

$$\gamma(s) = \sqrt{LC}\sqrt{(s+\sigma)^2 - \phi^2} \tag{2}$$

$$\sigma = \frac{1}{2}\left(\frac{R}{L} + \frac{G}{C}\right) \quad ; \quad \phi = \frac{1}{2}\left(\frac{R}{L} - \frac{G}{C}\right)$$

where the attenuation and phase constants are denoted as σ and ϕ, respectively, in terms of the line parameters per-unit length of the transmission line, respectively. As the line parameters are frequency dependent [1], the TW propagation velocity in a line is frequency dependent *i.e.* waves with different frequencies propagate at different velocities and attenuate at different rates. Being a step signal, the current TW theoretically contains an infinite spectrum of frequencies propagating at different velocities, resulting in distortion of the initial TW [25]. The wave propagation in the line is characterized by $e^{-\gamma(s)x}$. $I_{st}(s)$ being the Laplace transform ($\mathcal{L}$) of current step signal, the distorted current signal resulting after propagation of distance x can be expressed in Laplace domain as,

$$i_I(x,s) = e^{-\gamma(s)x} I_{st}(0,s) \tag{3}$$

where $i_I(x,s)$ is the distorted signal incident at the relay location. As long as there is no transition, the step wave propagates in the line as described by (3). When a transition point is encountered, reflected waves are generated, and the relay records the total of incident and reflected TWs, described in time domain by [1]

$$i(x,t) = \mathcal{L}^{-1}\left[(1+\rho) i_I(x,s)\right] \tag{4}$$

where $i(x,t)$ is the TW recorded by the relay, ρ is the current reflection coefficient. From (3), for a small value of x, $i(x,t)$ is a step signal, which is distorted more as x increases. This work utilizes the distortion level introduced by the line on the current TW to identify faults in the zone of protection.

2.2. Traveling wave extraction

The signal processing for TW extraction is provided in Fig. 1. The current signals from current transformer(CT) secondaries are filtered in an analog anti-aliasing filter (AAF), and then each signal is sampled at 1 MHz through an analog-to-digital converter (ADC). The raw samples of current are used to extract the TWs by passing through band-pass, and the differentiator–smoother (DS) filters [10,24]. The band-pass filtering avoids power frequencies (50 Hz and harmonics) and high frequencies to eliminate the noise components. The TWs are extracted using a DS filter with half of the filter coefficient values being $-h$, and the rest set to h. The filter coefficients $h(l)$ are chosen so that $h = 2/N$, for unity gain of step-signals, where N is the number of filter coefficients [10]. The extracted current TW samples (i_{TW}) are obtained as,

$$i_{TW}(k) = \sum_{l=1}^{N} h(l) i(k - N + l) \tag{5}$$

The shapes of the waves are obtained inherently in the TW extraction process [24].

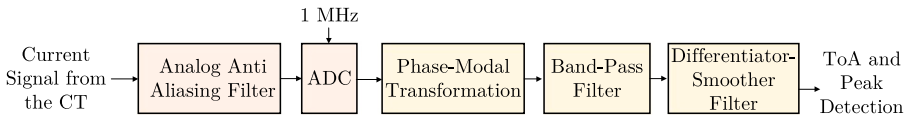

Fig. 1. Signal processing flow for TW extraction in the proposed method.

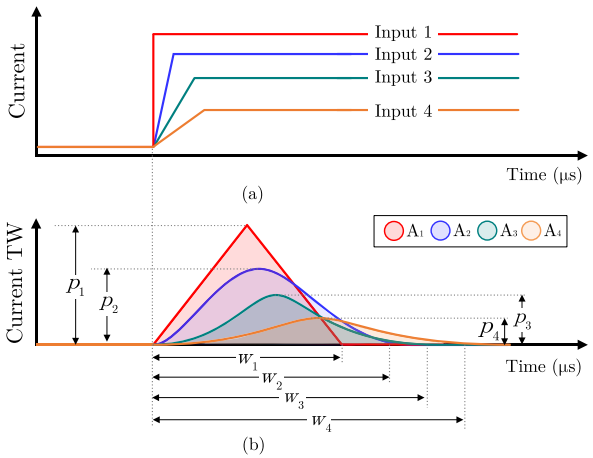

Fig. 2. (a) Input signals, and (b) obtained TWs for different attenuation levels.

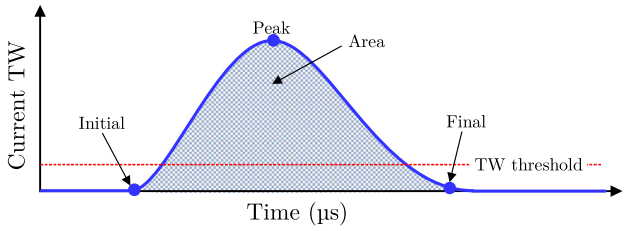

Fig. 3. Demonstration for area and peak calculation.

2.3. Waveshape analysis

The current signals with different distortion levels and the corresponding outputs of the DS filter are shown in Fig. 2(a) and (b), respectively. A triangular output with unitary gain can be observed for the ideal step change in the signal (input 1). The area (A_1) enclosed by this triangular waveshape can be expressed as,

$$A_1 = \frac{1}{2} p_1 w_1 \tag{6}$$

where p_1 and w_1 are the peak and width of the waveshape, respectively.

With an increase in the fault distance, the distortion level in the step-change increases. Input 2, 3 and 4 in Fig. 2(a) are the current TWs with increasing distortion levels. In the DS filter, these distorted signals result in parabola-shaped outputs where the peak magnitudes decrease, and the width of the waveshape increases for higher distortion levels [10,24,26]. The areas enclosed by these parabolic waveshapes ($A_{\{2,3,4\}}$) can be obtained as,

$$A_{\{2,3,4\}} = \frac{2}{3} p_{\{2,3,4\}} w_{\{2,3,4\}} \tag{7}$$

where $p_{\{2,3,4\}}$, and $w_{\{2,3,4\}}$ are peak and width, respectively, of the corresponding waveshapes 2, 3 and 4.

For a transmission line, the peak of the wave depends on the fault resistance, fault inception angle (FIA), and the traveled distance that causes attenuation [21]. The width of the wave depends on the dispersion level caused due to the distance covered by the TW [1]. With an increase in fault distance (Input 1 to 4), the widths of the waveshapes increase.

$$w_4 > w_3 > w_2 > w_1 \tag{8}$$

Eq. (8) can be represented in terms of (6) and (7) as,

$$\frac{A_4}{p_4} > \frac{A_3}{p_3} > \frac{A_2}{p_2} > \frac{A_1}{p_1} \tag{9}$$

Thus, the ratio area/peak increases with the width of the wave. In addition, the distortion level is better characterized by area/peak than the width of the waveshape as the shape changes from triangular to parabolic. Thus, in this work, the ratio area/peak (hereinafter, termed as Λ) is utilized as a measure to approximate the fault distance from the line end.

3. Proposed method

The features from the waveshape of extracted current TW, like area and peak, are utilized in this work to formulate a single-ended data-based technique to identify internal faults in the transmission line. As in (9), Λ increases with the fault distance, and thereby, fault in the protected zone can be identified by setting a threshold (Λ_{th}) for it. Λ_{th} is set based on the Λ for the protected zone. The decision is also supervised by a directional element to ensure a fault in the protected line. The procedure for calculation of Λ, protected zone setting, and overall description of the proposed method is provided below.

3.1. Estimation of the ratio area/peak

Fig. 3 depicts the area and peak calculation process for the current TW. Once current TW exceeds the threshold, peak (p) is obtained by interpolation method using a few samples of current TW before and after the peak. Then, the area under the waveshape with the x-axis (current TW = 0) is obtained using the trapezoidal rule as

$$A = \sum_{z=int.}^{z=fin.} i_{TW}(z)\Delta t \tag{10}$$

where $int.$ and $fin.$ correspond to the initial and final samples when the current TW is greater than 0 (current TW > 0). Δt is the time step between two consecutive samples. Λ is obtained using the area (A) and peak (p) of current TW.

3.2. Threshold for fault identification in the protected zone

Considering the uncertainties in line parameters, non-ideal filtering process and numerical errors in area and peak calculation, the protected zone(PZ) boundaries are set at 95% of the total line length. If the uncertainties in the line parameters and line lengths are higher, then the zone boundary can be further reduced to 90% or lower. A lower threshold improves security against external faults and reduces the reach, while a higher threshold provides an increased reach but reduces the security against external faults. A suitable zone boundary can be chosen considering the uncertainty level in the line parameters. The PZ boundary is similar to zone-1 in the conventional distance relays. The steps for threshold setting on Λ for the identification of a fault in the protected zones are as follows:

1. The distortion introduced by that protected zones of the line on a step wave is obtained using γ and PZ as in (3) and (4) [27].

Table 1
Termination impedances of different network elements.

Element	Inductor (L)	Capacitor (C)	Transformer	Transmission line (L,C)
Termination impedance	Ls	1/Cs	∞	L/C

2. The reflection coefficients for different type of terminations are given in Table 1 [1].
   The transmission lines are terminated with various capacitive and inductive elements, such as reactors, transformers, capacitor banks and other transmission lines. The equivalent termination impedance(Z_T) considering all the connected elements are obtained. The current TW reflection coefficient can be calculated using Z_T and the characteristic impedance of the protected line (Z_c) as:

$$\rho = \frac{Z_c - Z_T}{Z_c + Z_T} \tag{11}$$

3. The distorted signal, as obtained in (4), is convoluted with the digital bandpass filter followed by DS filter coefficients as in (5), and the current TW samples are obtained.
4. The Λ of the corresponding TW samples obtained using (5) is set as the threshold Λ_{th} for identification of faults in the protected zone.

Further, In practical applications, line energization maneuvers are performed to measure the distortion on the actual TW during propagation in the protected line [24,26]. The measured Λ of the distorted waveshape is utilized for threshold setting for internal fault identification.

3.3. Directional supervision

The directional element, as described in the literature [28] is used for directional supervision. The polarities of prefault modal voltage and modal current TWs are utilized to identify the fault direction. The same polarity of the prefault voltage and current TW indicates a forward fault, and opposite polarities indicate a reverse fault. The direction thus obtained locally is used for internal fault identification, with the condition that an internal fault must be in the forward direction of the relay.

3.4. Overall description of the proposed protection method

Fig. 4 shows the logic of the proposed protection method, where internal fault identification routines are processed. The current TWs are extracted as per the steps depicted in Fig. 1. When the current TW exceeds a set threshold a fault event is identified and Λ is estimated as described in Section 3.1. If $\Lambda < \Lambda_{th}$ a fault in the protected zone (PZ) is identified, which is supervised by a local directional element [28] only at the corresponding end relay to ensure an internal fault in the protected line. The trip command is generated for internal faults.

Direct underreach transfer trip (DUTT) scheme as in Fig. 4(b) is suitable to accelerate the trip decision and isolate the line from both ends in case of internal faults. In the DUTT scheme, if the local relay identifies a fault as internal to the line, it communicates a trip signal to the remote end, where the breaker is tripped without any additional qualification.

Table 2
Performance for different fault locations from relay M.

Fault	Section	FL (km)	Λ_M (μs)	Direction	Relay decision
Internal	2–3	10	10.01	Forward	Internal
	2–3	75	10.80	Forward	Internal
	2–3	140	11.70	Forward	Internal
External	3–4	170	12.38	Forward	External
	1–2	30	10.33	Reverse	External

4. Results

Simulations are performed in the 400 kV test system of Fig. 5(a) in PSCAD/EMTDC [29] to assess the validity of the proposed method. Frequency-dependent (phase) models with the tower configuration as illustrated in Fig. 5(b) are used to represent the transmission lines. The TWs are extracted through the DS filter with 20 coefficients ($N = 20$) having values −0.1 for one half ($N/2$) and 0.1 for another half number of coefficients. Aerial-mode (alpha and beta-mode) current TWs are considered for the evaluation of the proposed method. The aerial-mode characteristic impedance (Z_c), propagation velocity (v) and the length (l) of the protected line (Bus 2–3) are 422 Ω, 292 m/μs and 150 km, respectively, for the signal frequency of 20 kHz. The threshold for current TW detection is set as 10 A to eliminate low-energy events. Considering the uncertainties in line parameters, non-ideal filtering process and numerical errors in area and peak calculation, the protected zone boundaries are set at 95% of the total line length. The threshold Λ_{th} is determined as in Section 3.2 for a fault at the zone boundary (142.5 km) and set as 11.85 μs. The proposed method is tested for various fault parameters and measurement noise level as follows.

4.1. Performance with different fault locations

AG faults with $R_f = 1$ Ω are simulated at 10 km, 75 km and 140 km from bus 2 in the line section 2–3 with 90° FIA. The corresponding waveshapes of current TWs are shown in Fig. 6. With the increase in the fault distance, attenuation and dispersion in the waveform also increase. The area/peak values calculated at relay-M (Λ_M) for these fault scenarios are presented in Table 2. For faults close to the relay, the waveshape is triangular (Fig. 6) and $\Lambda_M \approx 10$ μs, which is half of the DS filter length. Upon increasing, the fault distance Λ_M increases and approaches Λ_{th} for faults near the zone boundary. Comparing Λ_M and Λ_{th}(= 11.85 μs), the fault cases are identified to be within the zone boundary of the protected line. The directional element at relay-M confirms the faults to be in the forward direction. Therefore, the fault cases are correctly identified to be within the protected line section 2–3 using local data.

During the fault on the line section 3–4, 170 km from bus 2, the calculated Λ_M by relay M exceeds the threshold Λ_{th}. The proposed method identifies the fault to be external to the protected zone using local data. For the fault simulated at a distance of 30 km from bus-2 on the line section 1–2, $\Lambda_M < \Lambda_{th}$; however, the directional element at relay-M sees it as a reverse fault. The relay correctly identifies both faults as external to the protected zone using the proposed method. Thus, the proposed method is found dependable for internal faults and secure for external faults occurring at different locations.

4.2. Performance for different fault inception angles

Solid AG faults with FIA 5°, 10°, 30°, and 90° are simulated at 140 km from relay M. The obtained Λ_M in such conditions is summarized in Table 3. Variations in fault locations result in distinct magnitudes of TWs at the fault point. Upon initiation, TWs experience changes in waveform distortion influenced by the distance they traverse along the line. Therefore, for a given fault location, the distortion level in the wave shape at the relay is the same, even with different FIAs. From

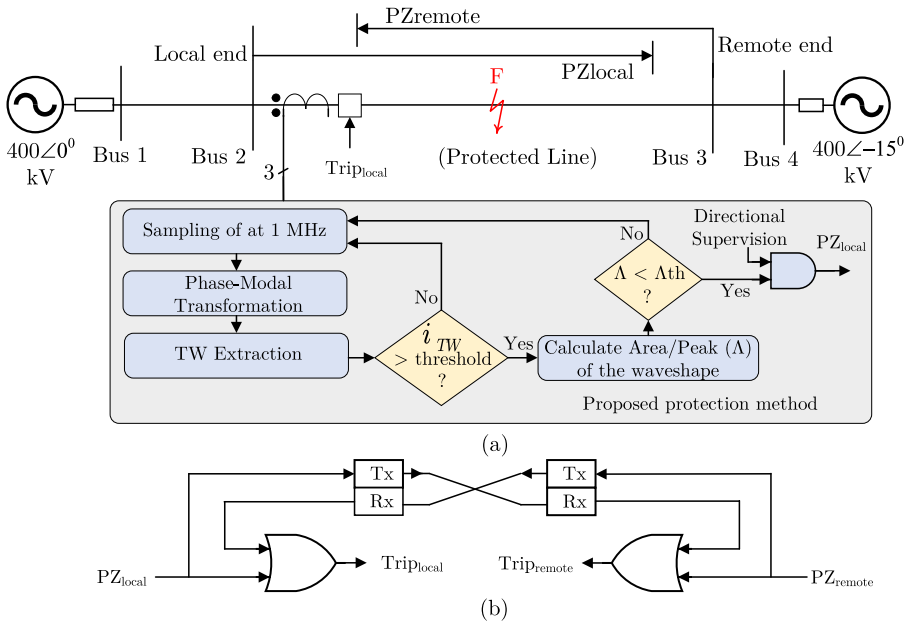

Fig. 4. (a) Protection logic of the proposed method (b) direct underreach transfer trip scheme.

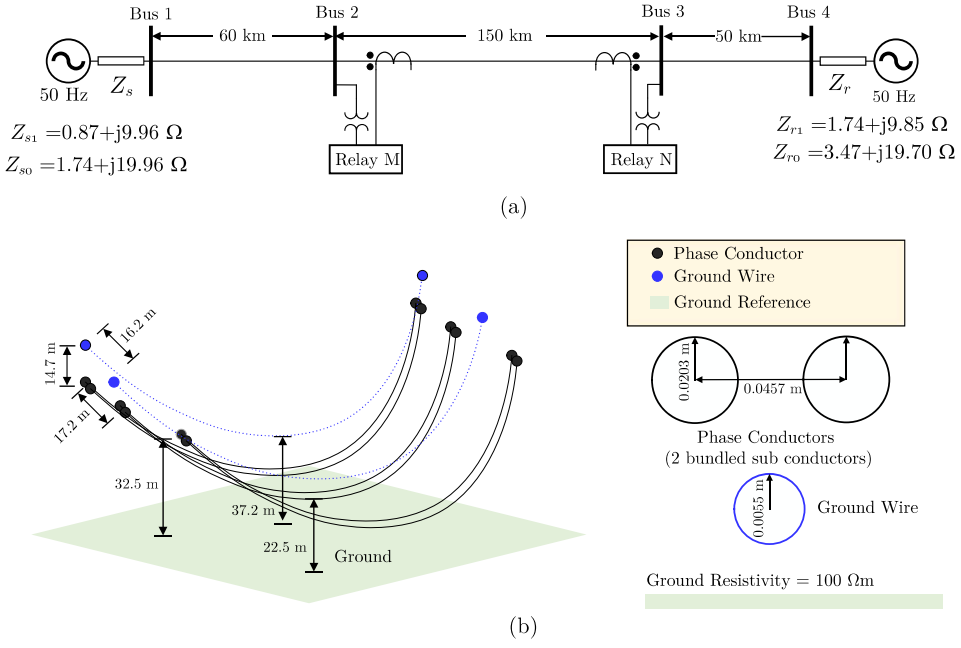

Fig. 5. (a) A 400 kV test system under study and (b) the physical configuration of transmission line.

Table 3
Performance for different fault inception angles.

Fault	Section	FL (km)	FIA (°)	Λ_M (μs)	Direction	Relay decision
Internal	2–3	140	5	11.70	Forward	Internal
			10	11.70	Forward	Internal
			30	11.70	Forward	Internal
			90	11.70	Forward	Internal
External	3–4	170	5	12.38	Forward	External
			10	12.38	Forward	External
			30	12.38	Forward	External
			90	12.38	Forward	External

Table 3, Λ_M remains nearly constant for faults at a given location even with different FIAs. The proposed feature being less affected by the variation in FIA, the proposed method correctly identifies all the internal faults for variation in fault inception angle.

External faults with different FIAs are simulated at 170 km from relay M. The obtained Λ_M (Table 3) for different FIAs are nearly equal. Thus, the proposed method identifies the fault case as external even with variations in FIA, which is correct.

4.3. Performance with different fault resistances

The assessment of the proposed method's effectiveness involves the simulation of AG faults at various fault resistance levels: 0 Ω, 10 Ω, and

Table 4
Performance for different fault resistances.

Fault	Section	FL (km)	R_f (Ω)	Λ_M (μs)	Direction	Relay decision
Internal	2–3	140	0	11.70	Forward	Internal
			10	11.70	Forward	Internal
			100	11.70	Forward	Internal
External	3–4	170	0	12.38	Reverse	External
			10	12.38	Forward	External
			100	12.38	Forward	External

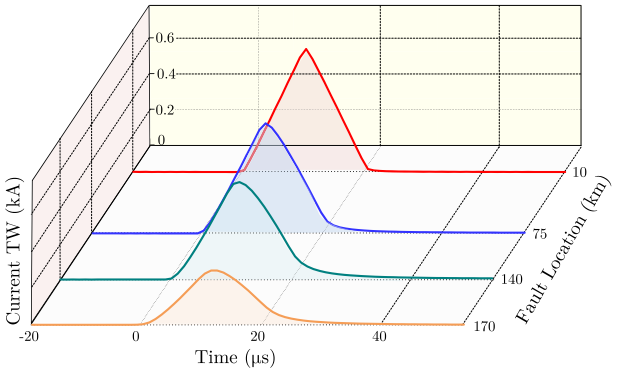

Fig. 6. Shape of current TWs obtained for different fault locations.

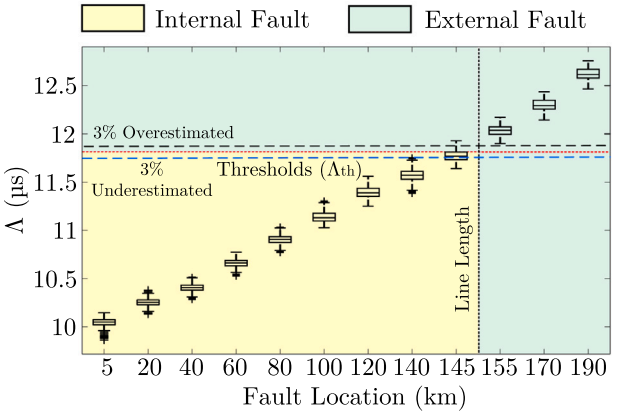

Fig. 7. Variation of area/peak with the fault location for faults with variation in location, resistance, FIA and type.

100 Ω. These simulations are conducted at 140 km from relay M, with FIA = 90°. The results can be found in Table 4. The increase in fault resistance leads to a reduction in the magnitude of the TW generated at the fault location. Once the TW is launched, the distortion in the waveshape depends on the TW propagation through the line. Therefore, for a specific fault location, Λ_M values remain nearly unique despite varying fault resistances. Using the Λ_M and fault direction, relay-M correctly identifies the faults as internal to the protected line.

External AG faults with R_f = 0 Ω, 10 Ω and 100 Ω are simulated at 170 km from relay M. Table 4 shows that for external fault also Λ_M is nearly equal. Using $\Lambda_{th} < \Lambda_M$ and directional supervision relay-M correctly identifies the fault cases as external to the protected line.

4.4. Large scale analysis

The method is tested for a large number of fault cases constituting variations in fault location, resistance (R_f: 0, 1, 10, 30, 50, 100 Ω), inception angle (FIA: 10°, 30°, 60°, 90°, 120°, 150°, 210°, 270°, 330°, 350°), type (AG, BC, CAG, ABCG) and 40 dB measurement noise

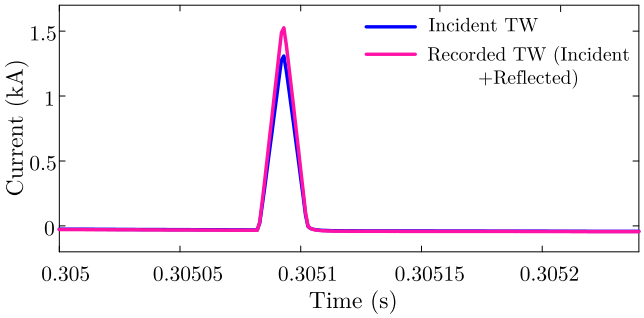

Fig. 8. Incident and recorded TWs at relay-M in presence of a transition point behind the protected line.

level. The obtained Λ at the relay at bus 2 are plotted in Fig. 7. Variation in fault resistance or inception angle causes a variation in the TW magnitude originated at the fault location. Once a TW of certain magnitude is launched, the distortion in the waveshape depends on the TW propagation through the line. For a particular fault location, the value of Λ remains nearly constant, regardless of the variations in fault resistance and inception angles. With increase in the fault distance the obtained Λ increases and exceeds Λ_{th} for faults external to the protected zone. Thus, using the waveshape information, internal and external faults in the protected zone are correctly identified.

Further, to evaluate the proposed method in the presence of line parameter uncertainty, the R, L, C parameters of the alpha-mode network are underestimated and overestimated by 3% [16] and the corresponding effect on threshold setting and internal fault identification is studied. For overestimation of the parameters, the threshold is 11.9, and for underestimation of the parameters, the threshold is 11.8 as shown in Fig. 7. With the underestimated and overestimated threshold settings, all the fault cases within 140 km are correctly identified as internal faults. The considered faults external to the line are correctly identified as external faults. The proposed method successfully identifies internal and external faults even with line parameter uncertainty.

4.5. Performance analysis with TW reflection at relay

The proposed method is assessed with a transition point behind the protected line. For the evaluation, the line 1–2 in the system of Fig. 5(a) is replaced by another line having a different characteristic impedance as that of line 2–3. A transmission line (frequency-dependent phase model) of characteristic impedance 305 Ω is connected between bus 1–2, which creates a transition point at bus 2. An AG fault of R_f = 0 Ω is created at FIA = 90° at a distance 25 km from bus 2. The current TW incident at the transition point and recorded by the relay are shown in Fig. 8. The shapes of both incident and recorded current TWs are triangular. The calculated value of Λ_M for both the current TWs is nearly equal to 10.38. The reflected TW modulates the peak of the recorded TW. However, the shape and Λ remain less affected because the reflected TW has a similar distortion level as on the incident TW caused by propagation in the line. This ensures that the proposed method is less affected by TW reflection at the relay location.

4.6. Comparative assessment

The existing TW-based distance functions identify the fault distance, $d = (u_\alpha - u_0)(\tau_\alpha - \tau_0)$, where u_α, u_0, τ_α, τ_0 represent the propagation velocities and arrival times of current TWs in the aerial and zero-mode, respectively [16]. Comparison is performed for a high resistance AG fault (R_f = 100 Ω) and low inception angles (FIA = 15°) at 75 km from bus 2 in the protected line. The measurement noise in the phase currents is considered as 40 dB SNR and the resulting alpha-mode and

Table 5
Area/peak obtained for inductive and capacitive terminations.

	Inductive				Capacitive			
	Internal		External		Internal		External	
	Without CT cable	With CT cable	Without CT cable	With CT cable	Without CT cable	With CT cable	Without CT cable	With CT cable
Area/Peak	34.5	34.4	35.5	35.4	35	34.9	35.7	35.6

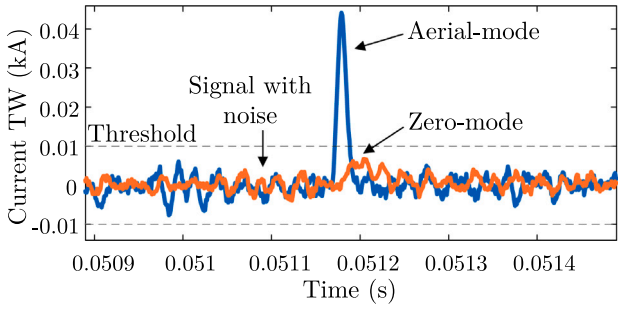

Fig. 9. Aerial and zero-mode current TWs for a high-resistance fault at low inception angle and 40 dB SNR measurement noise.

zero-mode current TWs are plotted in Fig. 9. The zero-mode TW is of significantly low magnitude (<TW detection threshold), which is not suitable for arrival time calculation and fault distance estimation. The existing approach remains indecisive. However, the aerial-mode current TW has sufficient magnitude and using the corresponding waveshape, $\Lambda = 10.95 < \Lambda_{th}$, and the proposed method correctly identifies the fault to be internal to the protected line. The proposed method outperforms the existing TW-based distance function for single-line-to-ground faults of high resistance and low inception angles. Further, the proposed method addresses all the fault types, while the existing method is limited to only ground faults.

5. Real-time validation

Real-time testing of the proposed method is performed on the RTDS Novacor simulator [30]. A test system with 4 buses, as shown in Fig. 10(a), is developed using the RSCAD FX 1.2 real-time software simulator in a substep environment, which allows the power system components to run in small time steps. The test system is simulated in parts with 3 different cores. Each of the cores simulates power system components and exchange data with 3.33 μs time-step (300 kHz). The TW extraction and proposed protection logic are modeled in substep 2 for the transmission line section 2–3 (150 km) with configuration shown in Fig. 10(b) (propagation time of 392 μs). The threshold Λ_{th} is set at 12.37 for the line section 2–3 for a fault on the zone boundary.

An internal B-g fault is simulated at 60 km from bus 2. The extracted TWs and estimated values of Λ at the local end (bus 2) and remote end (bus 3) are shown in Fig. 11. Comparing Λ and Λ_{th}, the fault is identified within the zone boundary at both ends. Therefore, an internal fault in the line section 2–3 is correctly identified by both the end relays. The estimated values of Λ at both local and remote ends for different fault locations is shown in Fig. 12. With the increase in the fault distance from the local end (Bus 2), the distortion effect in the waveshape is more prominent, and higher values of Λ are estimated. Comparing Λ_{th} and Λ, each of these faults is located in the protection zone. Here the trip decision is derived using the waveshape information at the corresponding relays.

External A-g faults have been applied to line section 3–4. Fig. 13 illustrates the estimated values of Λ in the relays at Bus-2 for faults occurring in line section 3–4. The estimated Λ at bus 2 relay exceeds the Λ_{th} threshold for faults in this specific line section. These faults occur outside the protection zone in all cases, the waveshape information accurately identifies them as external faults. Thus, the RTDS testing also validates the proposed approach.

6. Performance with CT secondary cables and different type of terminations

The proposed method has been tested for inductive and capacitive terminations, both with and without including CT secondary cables, using 400 kV, 50 Hz test systems as shown in Fig. 14.

Two systems were considered: one with an inductor and another with a capacitor present at the line termination, illustrated in Fig. 14(a) and (b), respectively. The equivalent models of CVT and CT, incorporating the secondary cables, are illustrated in Fig. 14(c) and (d), respectively. The CT secondary cable length is 100 m with the physical configuration as shown in Fig. 14(e). The CT secondary cables introduce high-frequency oscillations, called ringing in the current signal, at the CT secondary. In this work, the digital bandpass filter is used to reduce the effect of ringing in the current signal. The bandpass filter causes and additional tilting of the wavefront. For this system and filters used, the threshold on area/peak obtained for internal fault identification is 34.9 μs for inductive termination, and 35.3 μs for capacitive termination, considering 95% length of the protected line.

6.1. Performance with inductive termination

A single line to ground fault is created in the protected line at 140 km from bus 2 in the system of Fig. 14(a). The resulting current signals recorded with and without CT secondary cables are shown in Fig. 15(a). When CT secondary cables are included for simulation, high-frequency oscillations are observed, which needs filtering. Both the current signals are passed through a bandpass filter and the resulting signals are plotted in Fig. 15(b). After passing through the bandpass filter, the current signals with and without CT cables becomes identical. The TWs are extracted from the bandpass filtered current signals as shown in Fig. 15(c). The calculated area/peak of the waveshapes are provided in Table 5. By comparing the area/peak with the threshold setting, the fault case is correctly identified as internal even when the CT secondary cables are included for simulation.

An external fault is created in the line between bus 3 and 4 at 170 km from bus 2. The obtained shapes of the current TWs with and without the CT secondary cable are shown in Fig. 15(d). The obtained area/peak is provided in Table 5. Comparing the area/peak with the set threshold, the fault case is correctly identified to be an external fault.

6.2. Performance with capacitive termination

For capacitive termination, the waveshapes of an internal fault (at 140 km from bus 2) and an external fault (at 170 km from bus 2) are provided in Fig. 15(e) and (f), respectively. The area/peak of current TWs of both the fault cases are provided in Table 5. Using the threshold setting the internal and external faults are correctly identified.

To summarize, the CT cables introduce high-frequency oscillations in the current signals that needs filtering for TW extraction. In this work, the transients are filtered through a digital bandpass filter, followed by the TW extraction in the DS filter. The bandpass filter,

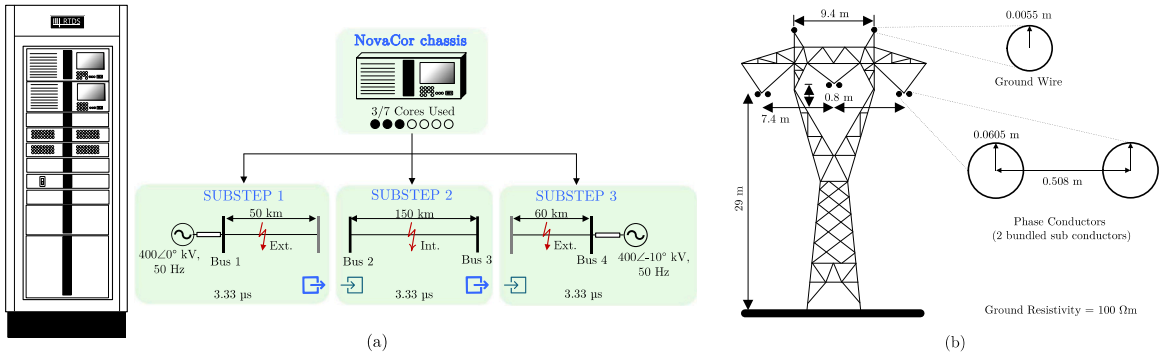

Fig. 10. (a) RTDS simulation setup, (b) transmission line configuration for the test system.

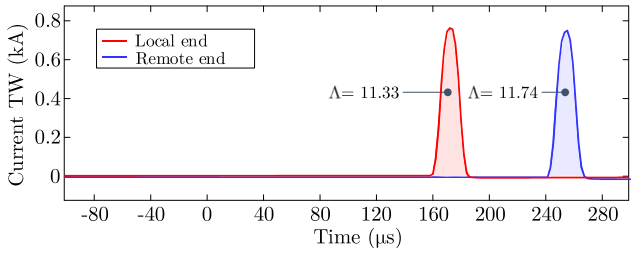

Fig. 11. Extracted TWs from RTDS simulation.

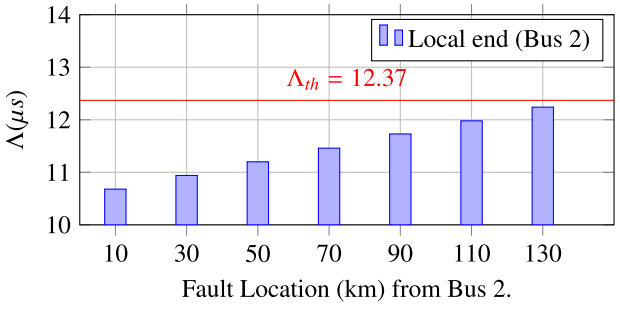

Fig. 12. Estimated values of Λ for internal faults at different locations.

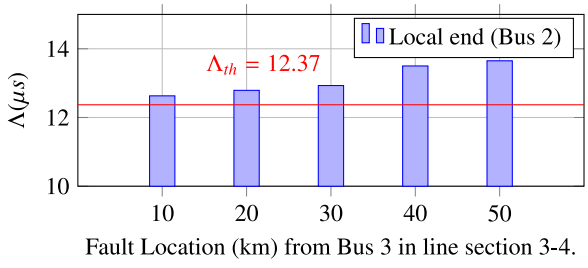

Fig. 13. Estimated values of Λ for external faults at different locations (line section 3–4).

causes additional tilting of the wavefront in the current signal, which is incorporated during the threshold setting.

The performance of the proposed method is tested including a reactor and capacitor at the protected line terminal. Thresholds are obtained by incorporating the termination impedance. Using suitable threshold settings based on the line termination, the internal and external faults are correctly identified.

7. Performance for close-in faults

The waveshape analysis for close-in faults have been performed with and without including the CT cable models in the system of Fig. 14(a).

An AG fault of $R_f = 0.1\ \Omega$ is created at 500 m from bus 2. The obtained alpha-mode current signals for the close-in fault are plotted in Fig. 16(a). The presence of CT cables introduce high-frequency oscillations in the current signal, which is suppressed by a bandpass filter as shown in Fig. 16(a). The current signals are passed through the bandpass filter and then the differentiator–smoother(DS) filter to extract the TWs. The obtained TWs are plotted in Fig. 16(b). It can be observed that when the CT cables are not included, the waveshape is nearly triangular, whose area/peak is 30.1 µs. When CT cables are included, the waveshape is slightly distorted; however, the area/peak = 30.5 µs, is slightly higher that of the triangular shape (see Fig. 16(b)). Using the threshold setting of 34.9 µs. The close-in fault is correctly identified to be internal to the protected line.

When faults occur close to the bus, a portion of the TW is reflected back from the bus towards the fault point depending on the termination impedance and oscillates between the bus and the fault point. With each reflection, the TW magnitude reduces and hence their effect on the initial waveshape decreases. Further, the reflected waves are less tilted because the propagated distance between the fault point and the bus is small. Therefore, nearly triangular waveshape is observed for close-in faults, when CT cable is not included. When the CT cables are included, the waveshape is not triangular; however, the associated area/peak remains identical to the triangular shape obtained without CT cable. In both the cases the close-in fault is correctly identified to be internal.

8. Discussion

In summary, the following contributions can be highlighted for the proposed method:

- The proposed method provides a current TW waveshape-based method for transmission line protection that simplifies the detection of internal faults in a line by using the peak and area under the waveshape of the initial current TW at the local end. This approach eliminates the need for complex computations and high-speed communication.
- The zone boundary is set based on the ratio of the area under the waveshape and its peak, which is less affected by the fault parameters which ensures fault detection, even for remote faults.

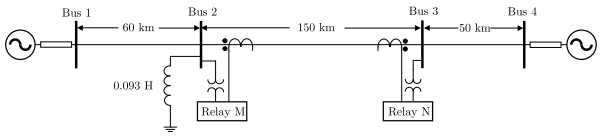

(a) A 400 kV test system with the line between bus 2 and 3 having inductive termination

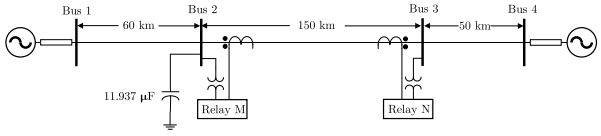

(b) A 400 kV test system with the line between bus 2 and 3 having capacitive termination

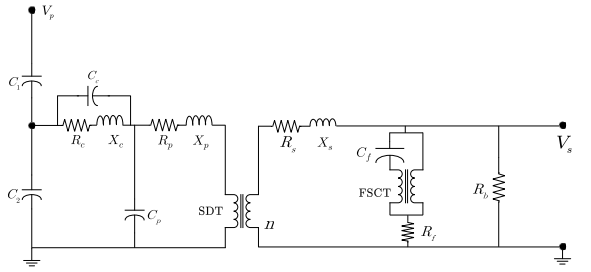

Voltage Divider:

$R_1 = 3310\ \Omega;\ C_1 = 1.6095$ nF
$R_2 = 59.0338\ \Omega;\ C_1 = 89.991$ nF

Compensating Circuit:

$R_c = 950.1\ \Omega;\ L_c = 67.92$ H

Stray Capacitances:

$C_p = 149.7$ pF; $C_c = 144.7$ pF; $C_{IW} = 149.7$ pF

Step-Down Transformer:

$R_p = 850.02\ \Omega;\ L_p = 4.443$ H
$R_s = 0.2467\ \Omega;\ L_s = 649.91\ \mu$H, n = 75.85

Ferro resonance Suppression Circuit:

$R_{f1} = 0.08\ \Omega;\ C_{f1} = 1565.38\ \mu$F
$R_{f2} = 1.2301\ \Omega;\ L_{f2} = 54.3$ mH
$R_f = 13.333\ \Omega$

Burden:

$R_b = 29.5\ \Omega;\ L_b = 98.2$ mH

(c) Equivalent model of the CCVT considered

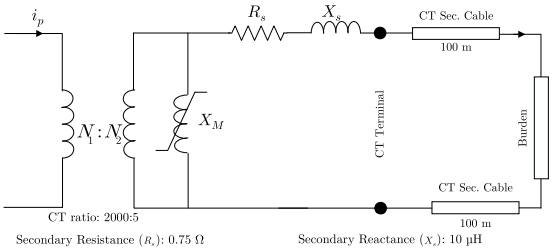

Secondary Resistance (R_s): 0.75 Ω
Secondary Reactance (X_s): 10 μH
Non-linear Core (X_M) Characteristics:
Burden Impedance : 0.5+ j 0.251 Ω

I	0.0198	0.0281	0.0438	0.0565	0.0694	0.1025	0.2167	0.7002	1.0631	15.903
ψ	0.2851	0.6040	1.1141	1.5343	1.8607	2.2771	2.6522	3.0234	3.1038	3.2261

(d) Equivalent model Of the considered CT with cable length of 100 m.

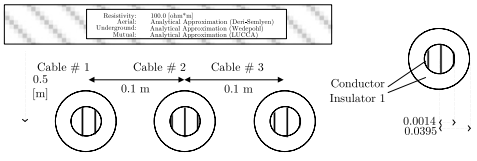

(e) Physical configuration of the CT secondary cable.

Fig. 14. Test system configurations for evaluating the proposed method across various line terminations.

- Moreover, the proposed method only uses initial waves, avoiding the issue of discriminating reflected TWs from fault point or line terminals. This aspect, along with avoiding accurate information on the arrival time, addresses the practical challenges associated with data synchronization at high sampling rates.
- Only aerial-mode signals are used for decision making, therefore the proposed method is applicable to all the fault types.

The practical lightning events cause significantly distorted waves and precursor transients, for which the decision should be avoided [24]. Lightning events can be distinguished from the fault events by monitoring the magnitudes of zero-mode and alpha-mode current TWs [3]. If the zero-mode magnitude is larger than the alpha-mode magnitude, that indicates a lightning event [3], and the corresponding decision can be avoided.

When the transmission lines are terminated in power transformers, they offer very high – ideally infinite – impedance to the high-frequency traveling waves [1,31]. If any other elements are connected to the protected line, the equivalent termination impedance becomes equal to the equivalent impedance of the other connected elements. Thus, having information of the connected elements at the line terminal, suitable thresholds on area/peak can be obtained for internal fault identification.

The CT secondary cables introduce high-frequency oscillations in the current signals, which is filtered out using a digital bandpass filter. The bandpass filtered current signal is used for successful identification of internal and external faults in the protected line.

9. Conclusion

This work proposes a current TW waveshape-based method for transmission line protection. The peak and area under the waveshape of the initial current TW at the local end are used to detect internal faults in a line. The zone boundary is set based on the ratio of the area under the waveshape and its peak. Fault distance estimation using such a feature is not altered by the fault resistance and fault inception angle. The proposed method uses only initial waves and thus overcomes the issue of discriminating reflected TWs from fault point or line terminals. The proposed method also does not require accurate information on the arrival time. The peak and area information of the waveshape accurately identifies the internal faults within the protected zone. Comparative analysis with available techniques highlights its effectiveness and advantages.

CRediT authorship contribution statement

Kuldip Nayak: Writing – original draft, Validation, Methodology, Conceptualization. **Soumitri Jena:** Writing – review & editing, Validation, Formal analysis. **Ashok Kumar Pradhan:** Writing – review & editing, Validation, Supervision, Conceptualization.

Declaration of competing interest

The authors declare that they have no known competing financial interests or personal relationships that could have appeared to influence the work reported in this paper.

Data availability

No data was used for the research described in the article.

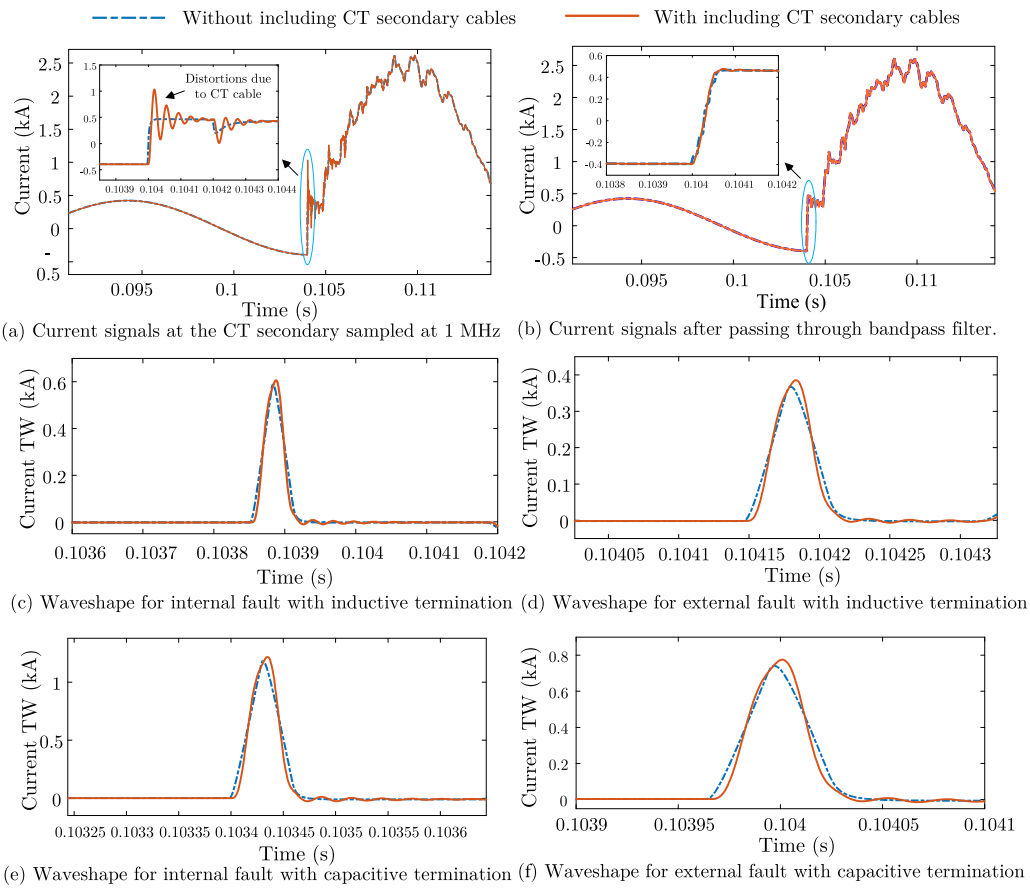

Fig. 15. The obtained current signals and current TWs for faults with different line terminations.

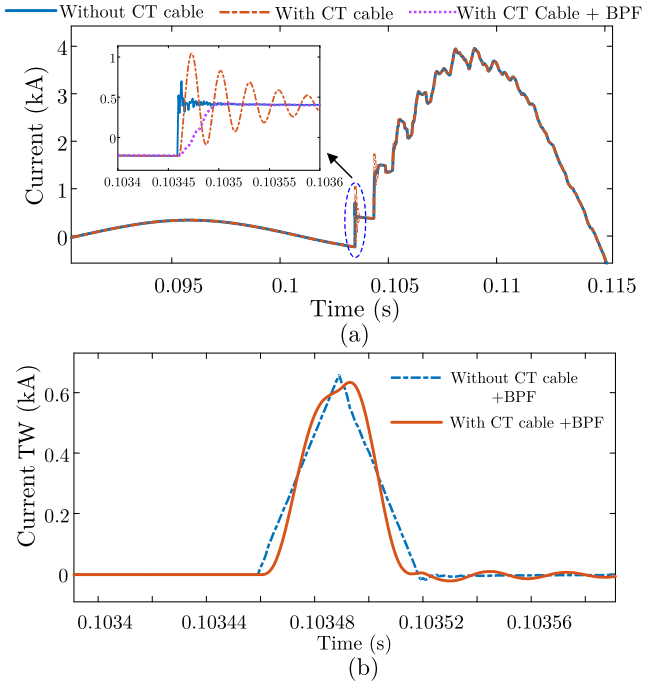

Fig. 16. (a) Current signals at the CT secondary, and (b) the extracted current TWs for a close-in fault.

References

[1] A. Greenwood, Electrical Transients in Power Systems, John Wiley & Sons, New York, NY (USA), 2013.

[2] F. Wilches-Bernal, A. Bidram, M.J. Reno, J. Hernandez-Alvidrez, P. Barba, B. Reimer, R. Montoya, C. Carr, O. Lavrova, A survey of traveling wave protection schemes in electric power systems, IEEE Access 9 (2021) 72949–72969, http://dx.doi.org/10.1109/ACCESS.2021.3080234.

[3] E.O. Schweitzer, B. Kasztenny, A. Guzmán, V. Skendzic, M.V. Mynam, Speed of line protection - can we break free of phasor limitations? in: 68th Annual Conference for Protective Relay Engineers, 2015, http://dx.doi.org/10.1109/CPRE.2015.7102184, College Station, TX, USA.

[4] J. Izykowski, E. Rosolowski, P. Balcerek, M. Fulczyk, M.M. Saha, Accurate noniterative fault-location algorithm utilizing two-end unsynchronized measurements, IEEE Trans. Power Deliv. 26 (2) (2011) 547–555, http://dx.doi.org/10.1109/TPWRD.2009.2031440.

[5] F. Costa, J.L. Júnior, M.A. Jahan, F. Lopes, K. Silva, K. Dantas, Low-sampling frequency two-terminal traveling wave-based overhead transmission line protection, Electr. Power Syst. Res. 224 (2023) 109639.

[6] L. Tang, X. Dong, S. Luo, S. Shi, B. Wang, A new differential protection of transmission line based on equivalent travelling wave, IEEE Trans. Power Del. 32 (3) (2017) 1359–1369, http://dx.doi.org/10.1109/TPWRD.2016.2568206.

[7] A. Lei, X. Dong, S. Shi, B. Wang, V. Terzija, Equivalent traveling waves based current differential protection of EHV/UHV transmission lines, Int. J. Electr. Power Energy Syst. 97 (2018) 282–289, http://dx.doi.org/10.1016/j.ijepes.2017.11.017, URL https://www.sciencedirect.com/science/article/pii/S0142061517323517.

[8] F. Namdari, M. Salehi, High-speed protection scheme based on initial current traveling wave for transmission lines employing mathematical morphology, IEEE Trans. Power Deliv. 32 (1) (2017) 246–253, http://dx.doi.org/10.1109/TPWRD.2016.2571341.

[9] F.V. Lopes, K.M. Silva, F.B. Costa, W.L.A. Neves, D. Fernandes, Real-time traveling-wave-based fault location using two-terminal unsynchronized data, IEEE Trans. Power Deliv. 30 (3) (2015) 1067–1076, http://dx.doi.org/10.1109/TPWRD.2014.2380774.

[10] F.V. Lopes, E. Leite Jr., J.P. Ribeiro, L. Lopes, A. Piardi, R. Otto, W. Neves, Using the differentiator-smoother filter to analyze traveling waves on transmission

lines: Fundamentals settings and implementation, in: International Conference on Power System Transients, 2019.
[11] R. Reis, F. Lopes, E. Ribeiro, C. Moraes, K. Silva, A. Britto, R. Agostinho, M. Rodrigues, Traveling wave-based fault locators: Performance analysis in series-compensated transmission lines, Electr. Power Syst. Res. 223 (2023) 109567.
[12] R.L. Reis, F.V. Lopes, Correlation-based single-ended traveling wave fault location methods: A key settings parametric sensitivity analysis, Electr. Power Syst. Res. 213 (2022) 108363.
[13] J.L. Júnior, F. Costa, F. Lopes, Two-terminal traveling-wave-based non-homogeneous transmission-line protection, Electr. Power Syst. Res. 223 (2023) 109622.
[14] F.V. Lopes, R.L. Reis, K.M. Silva, Improving traveling wave-based transmission line fault location by leveraging classical functions available in off-the-shelf devices, IEEE Trans. Power Deliv. (2023).
[15] X. Dong, S. Luo, S. Shi, B. Wang, S. Wang, L. Ren, F. Xu, Implementation and application of practical traveling-wave-based directional protection in UHV transmission lines, IEEE Trans. Power Deliv. 31 (1) (2016) 294–302, http://dx.doi.org/10.1109/TPWRD.2015.2458933.
[16] R.L.S. França, F.C. Silva Jr., T.R. Honorato, J.P.G. Ribeiro, F.B. Costa, F.V. Lopes, K. Strunz, Traveling wave-based transmission line earth fault distance protection, IEEE Trans. Power Deliv. 36 (2) (2021) 544–553, http://dx.doi.org/10.1109/TPWRD.2020.2984585.
[17] E.P. Ribeiro, F.V. Lopes, K.M. Silva, A.G. Martins-Britto, Assessment of communication channel effects on time-domain protection functions tripping times, Electr. Power Syst. Res. 223 (2023) 109589.
[18] E. Ribeiro, F. Lopes, K. Silva, A. Martins-Britto, R.L. Reis, C.M. Moraes, R.L. Agostinho, M.A. Rodrigues, An interpolation-based solution to use low sampling rate records in traveling wave-based fault location methods, Electr. Power Syst. Res. 224 (2023) 109605.
[19] E.O. Schweitzer, B. Kasztenny, Distance protection: Why have we started with a circle, does it matter, and what else is out there? in: 71st Ann. Conf. for Prot. Relay Engineers, 2018, http://dx.doi.org/10.1109/CPRE.2018.8349791, College Station, TX, USA.
[20] O.D. Naidu, A.K. Pradhan, A traveling wave-based fault location method using unsynchronized current measurements, IEEE Trans. Power Deliv. 34 (2) (2019) 505–513, http://dx.doi.org/10.1109/TPWRD.2018.2875598.
[21] F.M. Demagalhaesjunior, F.V. Lopes, Mathematical study on traveling waves phenomena on three phase transmission lines part I: Fault-launched waves, IEEE Trans. Power Deliv. 37 (2) (2021) 1151–1160, http://dx.doi.org/10.1109/TPWRD.2021.3077769.
[22] R. Benato, S.D. Sessa, M. Poli, C. Quaciari, G. Rinzo, An online travelling wave fault location method for unearthed-operated high-voltage overhead line grids, IEEE Trans. Power Deliv. 33 (6) (2018) 2776–2785, http://dx.doi.org/10.1109/TPWRD.2018.2816067.
[23] O.D. Naidu, A.K. Pradhan, Precise traveling wave-based transmission line fault location method using single-ended data, IEEE Trans. Ind. Inform. 17 (8) (2021) 5197–5207, http://dx.doi.org/10.1109/TII.2020.3027584.
[24] E.O. Schweitzer, A. Guzmán, M.V. Mynam, V. Skendzic, B. Kasztenny, S. Marx, Locating faults by the traveling waves they launch, in: 67th Annual Conference for Protective Relay Engineers, 2014, http://dx.doi.org/10.1109/CPRE.2014.6798997, College Station, TX, USA.
[25] Y. Hase, Handbook of Power System Engineering, John Wiley & Sons, Chichester, England, 2007.
[26] A. Guzmán, B. Kasztenny, Y. Tong, M.V. Mynam, Accurate and economical traveling-wave fault locating without communications, in: 2018 71st Annual Conference for Protective Relay Engineers, CPRE, 2018, pp. 1–18, http://dx.doi.org/10.1109/CPRE.2018.8349768.
[27] B. Gustavsen, J. Sletbak, T. Henriksen, Calculation of electromagnetic transients in transmission cables and lines taking frequency dependent effects accurately into account, IEEE Trans. Power Deliv. 10 (2) (1995) 1076–1084.
[28] K. Nayak, S. Jena, A.K. Pradhan, Travelling wave based directional relaying without using voltage transients, IEEE Trans. Power Deliv. 36 (5) (2021) 3274–3277, http://dx.doi.org/10.1109/TPWRD.2021.3099338.
[29] Manitoba HVDC Research Centre, PSCAD ver. 4.6, Electromagnetic Traransients including DC (EMTDC, Software Package), Winnipeg, MB, Canada.
[30] RTDS NovaCor Simulator, RTDS Technologies Inc., Winnipeg, MB-CANADA, URL https://knowledge.rtds.com/hc/en-us/articles/360034290474-NovaCor-.
[31] B. Kasztenny, M.V. Mynam, S. Marx, R. Barone, Traveling-wave overcurrent-a new way to protect lines terminated on transformers, in: 48^{Th} Annual Western Protective Relay Conference, 2021, virtual format.